A novel low-temperature fabrication approach of composite phase change materials for high temperature thermal energy storage

Qinghua Yu[a], Zhu Jiang[a], Lin Cong[a], Tiejun Lu[a], Suleiman Bilyaminu[a], Guanghui Leng[a], Zhentao Wu[b], Yulong Ding[a], Yongliang Li[a,1]

[a]Birmingham Centre for Energy Storage, School of Chemical Engineering, University of Birmingham, Birmingham B15 2TT, United Kingdom

[b]Aston Institute of Materials Research, School of Engineering and Applied Science, Aston University, Birmingham, B4 7ET, United Kingdom
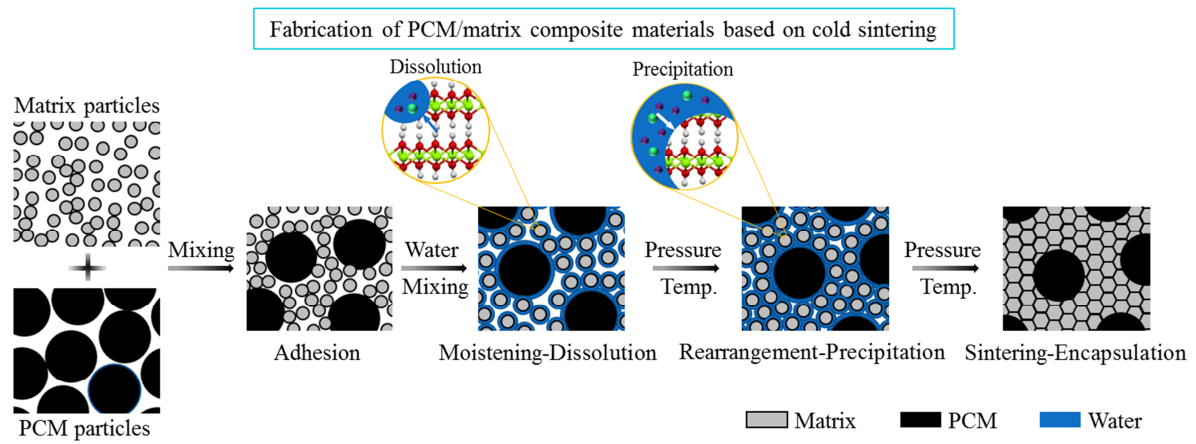
[1]Corresponding author. Tel.: +44 (0) 121 414 5135, Email: y.li.1@bham.ac.uk (Y. Li)

Abstract

Phase change materials (PCMs) are generally integrated into matrix materials to form shape-stabilized composite heat storage materials (HSMs) used for high temperature thermal energy storage applications. The conventional fabrication of composite HSMs is prevalently implemented at quite high temperatures, which is energy-intensive and narrows down the range of applicable PCMs because of thermal decomposition. Therefore, this paper establishes a novel fabrication approach to accomplish highly dense matrix to encapsulate PCMs at an extremely low temperature based on the recently developed cold sintering process. The feasibility of the proposed approach was demonstrated by a case study of $NaNO_3/Ca(OH)_2$ composite HSMs. It was observed that the $Ca(OH)_2$ matrix formed dense microstructure with obvious sintered boundaries and successfully encapsulated $NaNO_3$ as PCM. The HSMs maintained stable macroscopic shape after hundreds of thermal cycles, and exhibited an energy storage efficiency of 59.48%, little leakage of PCM, good thermal stability. Mechanical tests indicated that the HSMs possessed excellent mechanical properties when the sintering pressure is over 220 MPa. The discharging time of stored heat was presented through infrared thermography, and the heat storage capacity measured for the composite HSMs was over four times as high as those of typical solid storage materials of sensible heat, which demonstrated their decent heat storage performances. The HSMs can be used in the form of packed bed or parallel channel with multi-layered heat storage, which is benefit for efficiently utilizing solar heat and improving the performance of current energy storage system. This study provides a novel route for energy-saving and low-carbon fabrication of shape-stabilized composite HSMs.

Graphical Abstract

Fabrication of PCM/matrix composite materials based on cold sintering

Matrix particles

+

PCM particles

Mixing

Adhesion

Dissolution

Water
Mixing

Moistening-Dissolution

Precipitation

Pressure
Temp.

Rearrangement-Precipitation

Pressure
Temp.

Sintering-Encapsulation

☐ Matrix ■ PCM ■ Water

1. Introduction

High temperature thermal energy storage (HTTES) is expected to be one of the key enabling technologies for both the successful market introduction of large amounts of variable/intermittent electricity generation from renewable energy sources [1] and the energy saving and efficient energy utilization in conventional thermal systems and heat networks [2]. HTTES is also critical to improving the round-trip efficiency of recently developing compressed air energy storage (CAES) [3] and pumped thermal electricity storage (PTES) [4]. Cost-effective and high-performance heat storage materials (HSMs) are required for the above HTTES applications. Among various HSMs, latent heat based storage materials, also called phase change materials (PCMs), have attracted increasing attention because of high energy storage densities with nearly isothermal solid-liquid transition process [5]. The PCMs applicable for HTTES (such as molten salts and metals) exhibit high chemical corrosion in the liquid phase, especially for conventional metal containers [6]. Incorporating PCMs into suitable matrix or supporting materials to form shape-stabilized composite HSMs prove to be an effective strategy of overcoming chemical corrosion of PCMs, because the resulting composite materials can offer barriers to prevent leakage of liquid PCMs and avoid harmful reactions with surroundings even at elevated temperatures. Besides, the shape-stabilized composite HSMs enable direct contact heat transfer with working fluids, which is benefit for increasing the heat charging rate compared to conventional macro-encapsulation structures (i.e. pouring PCMs into containers) [7].

A multitude of studies have been devoted to high-performance shape-stabilized composite HSMs as well as novel fabrication methods in recent years [8]. Ge et al. [9] developed a composite materials consisting of a eutectic mixture of lithium and sodium carbonates as PCMs and MgO as a supporting material by uniaxial cold compression and high temperature sintering. The sintering temperature was up to 550 ℃ with holding time of

90 min. The supporting material underwent bonding process and hence formed a rigid microstructure during the sintering process, to maintain a stable shape and prevent leaking of PCMs during phase change. Qin et al. [10] formulated composite materials by the use of sodium sulfate as a PCM and diatomite as a structural skeleton material for shape stabilization. The formation process of composite materials also underwent uniaxial cold compression and high temperature sintering at 900 ℃ for an hour. They used the same method to fabricate $NaNO_3$/diatomite composite materials at a sintering temperature of 370 ℃ which held for an hour [11] and NaCl-KCl/diatomite composite materials at a sintering temperature of 680 ℃ which also held for one hour [12]. They stated that the melted PCMs were absorbed into the nanoscale pores of diatomite in the fabrication process to prevent their leakage. Similarly, the method of impregnating melted PCMs into porous materials has been used to fabricate various shape-stabilized composite HSMs [13]. Oya et al. [14] prepared erythritol-nickel composite HSMs by vacuum impregnation. It was proved that the porous nickel matrix offered a high effective thermal conductivity for the composite HSMs. Liu et al. [15] fabricated Na_2SO_4-mullite composite HSMs by infiltrating of the melted Na_2SO_4 into the pores of mullite. They found that the optimal temperature and duration of infiltration were 950 ℃ and 1 h, respectively. Nevertheless, the impregnation is usually incomplete even when additional vacuum is applied. It has been found experimentally that the risk of leakage can only be avoided for nano-pores (<20nm) [16]. But the nano-pores greatly inhibited the phase change behaviors of restricted PCMs, which led to enthalpies much less than theoretical values. Hierarchical porous structure or pore surface functionalization are thus required [17]. Besides, PCM microcapsules are considered one of promising shape-stabilized composite materials [18]. Nevertheless, most effects were devoted to microencapsulation of PCMs with a melting point under 100 ℃ [19]. It is technically more challenging to microencapsulate high-temperature PCMs. Nomura et al. [20] developed Al-Si alloy microcapsules covered by

α-Al$_2$O$_3$ shells, which were prepared in two steps including boehmite treatment and heat-oxidation treatment. In the heat-oxidation treatment process, the microcapsules needed to be heated up to 930 ℃ and kept at this temperature for 6 hours. However, the resulting PCM microcapsules had poor cyclic durability due to the low shell strength. The shell with low strength cannot bear the large stress caused by the volume expansion of PCM during its solid-liquid phase change and therefore easy to crack [21]. Nomura et al. [22] thus introduced a void into the core of the Al-Si alloy microcapsules to tolerate the volume expansion of PCM during phase change. In order to further increase the shell strength, they increased the temperature of heat-oxidation treatments from 930 °C to 1130 °C with duration of 6 h.

Although the above-mentioned shape-stabilized composite materials possess decent heat storage performance, their fabrication processes must undergo high temperatures for one hour or more. The required processing temperature should be higher than the melting points of PCMs at least or even higher. The high processing temperature complicates the fabrication with the high risk in thermal decomposition of PCMs and chemical reaction between different components [23]. A variety of PCMs with different melting temperatures are generally required to match various operating temperature ranges in the utilization of solar heat and industrial waste heat or their gradient utilization for realizing high-efficiency thermal storage [24]. Furthermore, combination of composite PCMs with different melting temperatures can form a multi-layered thermal storage device, which is helpful to reducing grade loss of the stored heat (exergy loss) and increasing the operating time [25]. Thermal decomposition of PCMs in the above-mentioned high temperature fabrication method severely limits the selectable range of PCMs in melting temperatures. For example, the LiNO$_3$/KCl mixture had a melting temperature of about 166 °C, while it was thermally decomposed at 315 °C according to the test of Huang et al. [26]. It implies that the LiNO$_3$/KCl cannot be used to prepare effective shape-stabilized composite HSMs through the

above-mentioned high temperature sintering or microencapsulation. In addition, the high temperature leads to substantial increase in energy consumption and the resulting composite materials are thus uncompetitive in cost [27]. Therefore, a cost-effective and high-efficiency fabrication approach of composite HSMs used for HTTES applications is urgently desired, which can broaden the selectable range of PCMs in melting temperatures simultaneously.

A sintering technology, namely the ''cold sintering process (CSP)'', is emerged very recently to achieve dense ceramics at incredibly low temperatures (<200 °C), by which a diverse range of chemistries and composites were successfully produced [28]. Basically the CSP uses water or aqueous solutions as a transient solvent to promote the densification by a mediated dissolution-precipitation process under a uniaxial pressure at a low temperature [29]. Such a low-temperature technology is hopeful to overcome the disadvantages of above-mentioned high temperature fabrication technology. However, this promising technology has not yet been applied to the fabrication of high temperature HSMs. More specifically, some key issues are not addressed in the literature: a) the feasibility of the CSP in the fabrication of composite HSMs; b) the underlying mechanism of CSP for the mixture of matrix materials and PCM; and c) the comprehensive heat storage performance of HSMs prepared by the approach based on CSP.

To fill the above knowledge gap, we develop for the first time a novel approach based on CSP to fabricate PCM-based shape-stabilized composite HSMs in this paper. Instead of incorporating liquid phase PCMs into the matrix or porous materials at high temperatures, composite HSMs were prepared by directly encapsulating solid state PCMs using dense matrix with the aid of CSP in the proposed approach. This approach abandons the conventional high temperature sintering and offers rapid formation of composite structure, and thus is cost-effective and high-efficiency. In the composite HSMs as an illustration prepared by the proposed approach, the NaNO$_3$ was used as PCM for thermal energy storage

while the $Ca(OH)_2$ acted as matrix to prevent the leakage of the PCM and maintain the shape stability of the composite HSMs. The microstructure, thermal properties, mechanical properties, thermal stability, chemical compatibility, thermal energy storage density of the prepared composite HSMs as well as the discharging time of thermal energy were characterized to demonstrate the feasibility of the proposed approach and reveal the underlying mechanism of the mixture of matrix and PCM. The potential applications of such shape-stabilized composite HSMs were also elaborated. This research will enrich the species of PCM-based shape-stabilized composite HSMs and open a novel perspective for energy-saving and low-carbon fabrication of composite HSMs based on the low temperature CSP.

2. Experimental method

2.1 Preparation

$NaNO_3$ and $Ca(OH)_2$ were purchased from Sigma-Aldrich, UK and all of analytical grade. $NaNO_3$ particles were firstly milled with a mortar and pestle, and sieved between 350 μm and 500 μm, whilst $Ca(OH)_2$ particles were milled and filtrated into superfine particles below 50μm. The two kinds of particles then were mixed with a weight ratio of 6:4 for CSP and the superfine $Ca(OH)_2$ particles automatically covered the surface of the large $NaNO_3$ particles in virtue of adhesion. The mixture particles were then mixed with 10 wt.% deionized water, which was homemade and introduced by spraying. Therein, the water uniformly moistened the particle surfaces and therefore dissolved the sharp edges of the particles, reducing the areas of particle-particle interfaces. The moistened particles were uniaxially hot-pressed in a steel die into dense pellets (15 mm in diameter and 2-4 mm in height) at 500 MPa and 120°C for 10 min. The die was preheated to 120°C for more than 1 h. With the aid of external uniaxial pressure, the $Ca(OH)_2$ particles as the matrix material rapidly rearranged yielding an initial compaction and the liquid phase fills the pores between

the particles; subsequently, the increase of temperature facilitated the evaporation of the water, which led to a fast epitaxial precipitation process on the surfaces of particles to bond adjacent particles and reach the final densification (sintering) of the matrix material $Ca(OH)_2$. Meanwhile, the $NaNO_3$ particles as the PCM were microencapsulated in the matrix material. Fig.1 presents a schematic illustration of the basic stages during CSP of composite HSMs. After the CSP the pellets were placed into an oven at 100°C for 2 h to remove residual water.

2.2 Characterization

The dried pellets were placed into a W-1000 thermal cycling test machine built in our lab to undergo cyclical heating-cooling between 270 °C and 350 °C with a heating/cooling rate of 10 °C. The macroscopic deformations of pellets after thermal cycling test were recorded by a common Canon camera. The microstructural and chemical studies for the pellets was performed using a scanning electron microscope (SEM, TM3030, Hitachi) equipped with an energy-dispersive X-ray spectroscopy (EDS) system to capture sintering and coating effects and confirm the components of the samples. The cross-sections of pellets were coated with a thin layer of gold by spraying to increase the resolution. The thermal properties including melting point, latent heat and specific heat were tested by using a differential scanning calorimeter (DSC, STAR^e system, Mettler Toledo) with a heating rate of 5 °C/min in a nitrogen environment. The specific heat was measured using sapphire as the reference substance. Thermal gravitational analysis (TGA) was performed in the thermal analyzer NETZSCH STA 449 *F3 Jupiter*® with a heating rate of 10 °C/min in a nitrogen environment to check the thermal stability. The phase structures were investigated with an X-Ray Diffractometer (XRD, X'Pert[3] Powder, PANalytical) with Cu Kα radiation to examine chemical compatibility. The sintered pellets were crushed into powders before DSC, TGA and XRD tests. The compressive strengths of the composite pellets at ambient temperature

were tested by a universal mechanical testing machine (LS100 plus, Lloyd Instruments). Thermal energy storage properties of pellets were captured by means of infrared thermography (VarioCAM® head HiRes 384, InfraTec).

3. Results and Discussion

3.1 Macroscopic and microscopic morphologies

The SEM images of as-prepared $NaNO_3$ particles and $Ca(OH)_2$ particles are shown in Figs. 2(a) and 2(b), respectively. It can be seen that the particle size of $NaNO_3$ is around 350–500 μm while that of $Ca(OH)_2$ is less than 50 μm. The SEM image of the mixture of the two types of particles is presented in Fig. 2(c). It shows that the $Ca(OH)_2$ particles adhere to $NaNO_3$ particles and form a layer to partially cover their surfaces. After spraying a certain amount of water on the surfaces of the mixture particles, as is shown in Figs. 2(d) and 2(e), the $Ca(OH)_2$ particles exhibit better adhesion on the surfaces of the $NaNO_3$ particles and the decent cohesion also occurs between $Ca(OH)_2$ particles, because of the hydrophilic property of the particles. Therefore, the preliminary core/shell-like structure is formed for further CSP with the aid of the sprayed water. The eventual cold-sintered composite pellet sample is presented in Fig. 2(f). Although the sample is cylindrical, the sample shape is changeable according to the shape of the used die.

The ability to maintain stable macroscopic shape of composite HSMs after undergoing thermal cycle tests is essential for enabling direct contact heat transfer. In order to reveal the macroscopic shape stability of $NaNO_3/Ca(OH)_2$ composite HSMs more clearly, another composite HSMs made of $NaNO_3$ as PCM and $CaCO_3$ as matrix were produced and tested using the same procedures and conditions. Fig. 3 shows the shapes of the two types of composite pellets at various sintering temperatures after 400-times thermal cycling between 270 ℃ and 350 ℃. All the $NaNO_3/Ca(OH)_2$ composite samples formed at various sintering

temperatures maintain their original cylindrical shapes as the same as that in Fig. 2(f) in spite of undergoing thermal cycling, while obvious collapse and deformation occur on all the $NaNO_3/CaCO_3$ composite samples. This can be explained as follows: The water solubility of matrix materials is crucial to the success of CSP when the water is adopted as transient solvent [30]. Since $CaCO_3$ is essentially insoluble in water while $Ca(OH)_2$ is slightly soluble in water, the $CaCO_3$ particles is hard to bond with each other via dissolution-precipitation process and eventually form stable dense structure like $Ca(OH)_2$ during the CSP. When the $NaNO_3$ wrapped by the $CaCO_3$ was melted, it leaked out from the $NaNO_3/CaCO_3$ composite pellet and the macroscopic shape of composite pellet was destroyed.

The $NaNO_3/Ca(OH)_2$ composite pellet after thermal cycling test was cut into two parts for observing inside microstructures from the cross-section. The microstructure and chemical element map of the $NaNO_3/Ca(OH)_2$ composite pellet are presented in Figs. 4(a) and 4(b), respectively. According to the identification of chemical elements obtained by EDS as shown in Fig. 4(b), the gray and black regions as shown in Fig. 4(a) are considered to be $NaNO_3$ and $Ca(OH)_2$, respectively. The composite configuration is manifested with the large $NaNO_3$ particles embedded into the superfine $Ca(OH)_2$ particles. In other words, $Ca(OH)_2$ particles form the perfect encapsulating effects to $NaNO_3$ particles. Figs. 4(c) and 4(d) display the enlarged microstructures of the local areas marked by the red and blue wireframes in Fig. 4(a) for better illustration, respectively. The two figures indicate that the $Ca(OH)_2$ particles are coalesced by an epitaxial growth based on precipitation triggered by the high pressure and rising temperature and apparent grain boundaries are subsequently formed between adjacent $Ca(OH)_2$ particles. Compared to Figs. 2(b-e), these substantial changes in the morphology of $Ca(OH)_2$ crystal indicate that the $Ca(OH)_2$ particles are sintered through the CSP and form dense microstructure. Therefore, from the holistic view, the $Ca(OH)_2$ matrix yields a 3-D network structure to increase the mechanical strength, avoid collapsing and maintain stable

shape of composite HSMs during the heating/cooling processes; from the view of single granular PCM (NaNO$_3$), the Ca(OH)$_2$ matrix forms a dense structure (i.e. shell) to encapsulate PCM particle and prevents it from leaking during the phase change processes. Darkwa et al. [31] proposed to axially press amounts of PCM microcapsules in a die into a non-deform heat storage composite pellets to improve their thermal conductivity and energy storage density. Wang et al. [32] also enhanced the thermal properties of PCM microcapsules through pressing with adding expanded graphite to form compact composite pellets. In their proposed studies, a complicated and low-efficiency PCM microcapsule synthesis process was inevitably involved. In contrast, the proposed method in the present study integrates the microencapsulation process and the pressure compaction process into one process, which is able to substantially elevate the fabrication efficiency and reduce the fabrication cost of the composite pellets including microencapsulating structures.

3.2 Thermal properties and thermal cycling performances

The DSC curves for NaNO$_3$/Ca(OH)$_2$ composite pellets containing 60 wt.% of NaNO$_3$ after different times of thermal cycling are shown in Fig. 5(a). The curve for pure NaNO$_3$ is also recorded in this figure for comparison. The curves for both the pure NaNO$_3$ and the composite material without thermal cycling contain a primary sharp endothermic peak and a secondary weak endothermic peak. The secondary peaks represent a solid-solid transition which occurs at almost the same temperature range of 250 ℃–280 ℃ for both the pure NaNO$_3$ and the composite material, whilst the primary peaks denote solid-liquid phase change (melting) which also takes place at almost the same temperature range of 290 ℃–320 ℃ for both the two materials. The peak temperatures at the two endothermic peaks are also nearly the same between the two materials. The melting latent heat of the composite material with 60 wt.% of NaNO$_3$ without thermal cycling is 102.8 J/g, whilst that of the pure NaNO$_3$ is

174.1 J/g. The former is approximately 60% of the latter. These preliminarily suggest good chemical compatibility between the components and good thermal stability, which are further confirmed by the following XRD and TGA analyses. The measured crystallization latent heats of the composite material and pure NaNO$_3$ are 106.5 J/g and 177.8 J/g, respectively. The energy storage efficiency (E_{es}) is usually used to represent the latent heat storage and release efficiency of the PCM-based composite material, which is defined as [33]

$$E_{es} = \frac{\Delta H_{m,comp.} + \Delta H_{c,comp.}}{\Delta H_{m,PCM} + \Delta H_{c,PCM}} \tag{1}$$

where $\Delta H_{m,comp.}$ and $\Delta H_{m,PCM}$ denote the melting latent heats of the composite material and pure PCM, respectively; $\Delta H_{c,comp.}$ and $\Delta H_{c,PCM}$ are the crystallization latent heats of the composite material and pure PCM, respectively. According to the calculation of Eq. (1), the as-prepared composite material achieved an E_{es} of 59.48%, indicating that it exhibited about 59% working efficiency compared to pure NaNO$_3$ under the same used mass. After undergoing thermal cycling, the two-peak structure of the DSC curves still exists. The detailed changes in melting temperature and latent heat with the times of thermal cycling are summarized in Fig. 5(b). The melting temperature of the composite material exhibited little change during the thermal cycling tests, which was always around 307 ℃ for different thermal cycle times. The latent heat of the composite material gradually decreased with the increase of thermal cycle times. After 400 thermal cycles, the latent heat of the composite material decreased by ~9.0% (from 102.8 J/g to 93.5 J/g). It should be mainly attributed to the leakage at the surface where some NaNO$_3$ particles were not well encapsulated. Since the un-encapsulated NaNO$_3$ particles became less due to leakage with the increasing cycle times, the decreasing trend of the latent heat became slower. From the 300 thermal cycles to 400 thermal cycles, the latent heat was almost unchanged.

3.3 Chemical compatibility and thermal stability

Fig. 6 demonstrates the XRD patterns of the $NaNO_3/Ca(OH)_2$ composite materials after different times of thermal cycling. The XRD patterns of the pure $NaNO_3$ and pure $Ca(OH)_2$ are also presented for comparative analysis. It can be seen from the XRD pattern (a) in Fig. 6 that the pattern of the sintered composite materials before thermal cycling contains only the patterns of pure $NaNO_3$ and pure $Ca(OH)_2$ and no new phase is observed, indicating excellent chemical compatibility between the PCM, matrix and water in the CSP or the fabrication process. By comparing the XRD patterns (a-c) in Fig. 6, it is found that all XRD peak positions of the composite materials are unchanged and no new peak is examined after different times of thermal cycling. It manifests that there is no chemical reaction between the PCM and matrix even at elevated temperatures, which further suggests excellent chemical compatibility between the components of the composite in its practical application temperature range. The experimental results also indicate that the intensities of XRD peaks of crystal planes at the position of $2\theta = 18.1$ and 34.1 for $Ca(OH)_2$ are slightly increased with the increase of thermal cycle times, while those at the position of $2\theta = 31.8$ and 39.0 for $NaNO_3$ are slightly decreased. It should be attributed to the slight change of weight ratio between the PCM and matrix during thermal cycling caused by little leakage of PCM.

The maximum operation temperature is one of the most important parameters for the use of composite HSMs in HTTES applications. It is typically determined by the thermal decomposition process of HSMs, which can be revealed by TGA. Fig. 7 presents the TGA curves of the pure $NaNO_3$, pure $Ca(OH)_2$ and $NaNO_3/Ca(OH)_2$ composite material. According to the TGA curves, the weight loss of pure $NaNO_3$ occurred via two-step degradation in the testing temperature range due to multiple thermal decompositions which is similar to the work of Gimenez et al. [34], while that of pure $Ca(OH)_2$ took place through one-step degradation caused by the dehydration reaction; for the $NaNO_3/Ca(OH)_2$ composite

material, the thermal decomposition process became more complicated, which integrated the thermal decomposition characteristics of pure $NaNO_3$ and pure $Ca(OH)_2$. The temperature at which 3% of initial weight of the sample has been lost is usually used to represent the maximum operation temperature or thermal decomposition temperature of the sample [35]. Accordingly, the thermal decomposition temperatures of pure $NaNO_3$, pure $Ca(OH)_2$ and $NaNO_3/Ca(OH)_2$ composite material can be obtained from Fig. 7, which are about 519.5 °C, 570.4 °C and 539.3 °C, respectively. The thermal decomposition temperature of the composite material is higher than that of pure $NaNO_3$, which confirms that the $Ca(OH)_2$ matrix slightly improve the thermal stability of $NaNO_3$. When the temperature is less than 500 °C, there is no weight loss for the composite material. In view of that the melting point of the composite material (about 307 °C) is much less than 500 °C, it can be claimed that the $NaNO_3/Ca(OH)_2$ composite material has excellent thermal stability in the potential application temperature range. When the composite material is used for configuring multi-layer thermal store with different melting temperature at different layers, the composite materials tend to operate in a quite narrow temperature near its melting temperature. In this case, the developed composite material has more safety allowance in thermal stability with respect to the designed operation temperature range.

3.4 Mechanical properties

The mechanical strength of the composite material is another important parameter for the practical use of composite HSMs, which can be examined by a compression process. The compressing curves of composite pellets produced at different sintering pressures are shown in Fig. 8(a). The thicknesses of pellets were controlled at around 3 mm for compressing tests and the extension rate of the squeeze head was set to 1 mm/min. It can be seen that the stress first increases and then decreases with the increase in the axial strain. The maximum stress is

corresponding to the 'rupture point', and thus the maximum stress can be referred to as compressive strength [12]. Both the measured compressive strength and the bearable maximum strain before rupture increase with the sintering pressure of the composite pellet. In addition, the stress of the pellet produced at a higher sintering pressure exhibits faster increasing rate with the increase in the axial strain, which implies that the increase of sintering pressure can elevate the Young's modulus or stiffness. More detailed variation of the compressive strength of the composite pellet with the sintering pressure is illustrated in Fig. 8(b). It shows that the increasing trend of compressive strength becomes quite slow when the sintering pressure more than 250 MPa. It can be inferred that the pellet has achieved decent sintering effects at the pressure of 250 MPa and thus further increase of sintering pressure cannot markedly increase its densification; when the sintering pressure is less than 250 MPa, the sintering effect or densification still has room for improvement. Even so, the compressive strength can be larger than 100 MPa when the sintering pressure is set to more than 220 MPa. Such compressive strengths demonstrate the excellent mechanical properties of the pellets produced in this study.

3.5 Thermal energy storage performances

In order to analyze the thermal energy storage performance of $NaNO_3/Ca(OH)_2$ composite HSMs, four composite pellets of the same weight (1.5 g) with different weight ratios of $NaNO_3$ were produced for comparison. The selected four weight ratios of $NaNO_3$ were 0% (pure $Ca(OH)_2$), 40%, 60% and 80%, respectively. The thermal energy storage density (D_{es}) of the composite pellets comprises the latent heat of PCM and the sensible heat of PCM and matrix, which can be calculated by the following equation [9]:

$$D_{es} = (1 - \varphi) \int_{T_s}^{T_e} c_{pms} dT + \varphi (\int_{T_s}^{T_{ms}} c_{pps} dT + \Delta h_m + \int_{T_{me}}^{T_e} c_{ppl} dT) \tag{2}$$

where φ is the weight ratio of the PCM in the composite pellet; c_{pms} is the specific heat of the matrix material that does not undergo phase change over the temperature range studied ($Jg^{-1}K^{-1}$) ; c_{pps} and c_{ppl} are the specific heat of the PCM in the solid phase and the liquid phase ($Jg^{-1}K^{-1}$), respectively; Δh_m denotes the melting latent heat (Jg^{-1}); T_s and T_e denote the starting and ending temperatures (K) of thermal energy storage process, respectively; T_{ms} and T_{me} represent the temperatures (K) at which the melting process of the PCM starts and ends, respectively. The obtained specific heats of the pure $Ca(OH)_2$ and pure $NaNO_3$ are illustrated in Fig. 9. According to Eq. (2) and the data in Fig. 9, Table 1 summarizes the calculated thermal energy storage densities of composite pellets with different weight ratios of $NaNO_3$ working over a temperature range of 140 °C–340 °C. Obviously, the thermal energy storage density notably increases with the weight ratio of $NaNO_3$. Specifically, the thermal energy storage density of the pellet with φ = 60% in the temperature range of 140 °C–340 °C increases by 57.4% compared to the pellet with φ = 0%.

The produced pellets with different energy storage densities were first placed into a furnace simultaneously and heated up to 340 °C for one hour. They were then taken out simultaneously and put in the air to cool down naturally. The instantaneous surface temperature distributions of the four pellets during the natural cooling process were recorded by means of infrared thermography. The resulting thermal images at different times are presented in Fig. 10(a-e). The central points at the upper surface of the pellets with $\varphi = 0$ %, 40%, 60% and 80% were marked as P1–P4, respectively. The photographing instant of the first image is regarded as initial time, i.e. t = 0 s, at which the temperatures of pellets are very close to each other. From the thermal images at other times, it can be seen that the larger the weight ratio of $NaNO_3$, the higher the pellet temperature. Specifically at t = 60 s, the temperatures at P1–P4 are 208.8 °C, 226.9 °C, 248.9 °C and 260.9 °C, respectively. It proves that the pellet with larger weight ratio of $NaNO_3$ still contained more heat energy with respect

to environmental temperature after the same time of natural cooling. It means that the pellet with larger weight ratio of $NaNO_3$ stored more heat energy during the heating process in the furnace. In view of the same mass for the four pellets, it is obvious that the pellet with larger weight ratio of $NaNO_3$ has higher thermal energy storage density in the same temperature rise, which coincides with the calculation in Table 1. In order to more clearly capture the temperature change characteristics of different pellets, the temperatures at P1–P4 were acquired by higher sampling frequency and are summarized as time-dependent temperature curves in Fig. 10(f). This figure manifests that pure $Ca(OH)_2$ pellet underwent distinct cooling effect compared to the $NaNO_3/Ca(OH)_2$ composite pellets. The temperature of pure $Ca(OH)_2$ pellet decreases nearly linearly over time, which is due to the fact that only heat conducting occurred inside the pure $Ca(OH)_2$ pellet during the cooling process. When the temperature at the any point of the $NaNO_3/Ca(OH)_2$ composite pellet decreases below its own solidification point, the composite pellet initiated release of latent heat and keep itself in a narrow phase change temperature range, then a simple heat conducting occurred when the temperature of the entire pellet decreased below its own solidification point. Therefore the temperature change curve of each $NaNO_3/Ca(OH)_2$ composite pellet contains a segment with extremely low decreasing rates. The time span of such a segment increases with the weight ratio of $NaNO_3$. Specifically, the duration time of the nearly isothermal heat release process is about 16 seconds for the pellet with $\varphi = 60\%$ in the natural cooling condition. The duration time for the pellet with $\varphi = 80\%$ is slightly longer than that for the pellet with $\varphi = 60\%$ and is not as long as expected, which is resulted from the larger leakage of PCM in the former pellet. The discharging times of thermal energy within the four pellets from about 323 ℃ to 140 ℃ at the natural cooling condition are summarized in Table 1. It can be seen that the $NaNO_3/Ca(OH)_2$ composite pellets maintain longer discharging process of thermal energy compared to the pure $Ca(OH)_2$ pellet in the same temperature drop and the discharging time

increases with the weight ratio of NaNO$_3$. These results demonstrate that the fabricated composite pellet possesses excellent thermal energy storage performances, because the PCMs successfully encapsulated inside matrix can absorb, store and release amounts of latent heat in a nearly isothermal phase transition process. In light of this, the method based on CSP proposed in this paper is an effective ways to fabricate shape-stabilized composite HSMs.

3.6 Potential applications of shape-stabilized composite HSMs

From the above, the PCM-based composite HSMs prepared by the proposed approach in this study showed high heat storage density, good thermal stability, long cyclic durability, decent mechanical strength and excellent shape stability at elevated temperatures. Hence, the shape-stabilized composite HSMs can be used as an alternative for various HTTES applications, to substitute the conventional solid sensible heat storage materials, such as Fe$_3$O$_4$ and quartzite. McTigue et al. [36] and He et al. [37] adopted Fe$_3$O$_4$ and quartzite as heat storage mediums to improve the overall performances of PTES and CAES systems, respectively. Table 2 compares the heat storage capacity of the composite HSMs prepared in this work with those of Fe$_3$O$_4$ and quartzite in the same temperature range of 290 ℃−340 ℃. It was assumed that the specific heats of Fe$_3$O$_4$ and quartzite were constant in the calculated temperature difference of 50 ℃. It can be seen from Table 2 that the prepared composite HSMs offer more than four times the mass-based heat storage density of the two typical solid sensible heat storage materials. Meanwhile, the volume-based heat storage density of composite HSMs is 1.7 times higher than that of Fe$_3$O$_4$ and 3.5 times higher than that of quartzite. In view of the higher energy storage capacity, using the prepared composite HSMs to replace Fe$_3$O$_4$ and quartzite as heat storage mediums is capable of remarkably reducing the weight and volume of PTES and CAES systems.

The expected application strategies of the PCM-based shape-stabilized composite HSMs are illustrated in Fig. 11. One strategy is packed bed as shown in Fig. 11(a). The prepared composite pellets are stacked in the multilayer packed bed. Different layers can adopt same composite pellets or different pellets with different PCMs. The packed bed of same composite pellets is similar to the conventional packed bed of Fe_3O_4 or quartzite, but the former provided much higher heat storage capacity. For the packed bed using different pellets at different layers, the melting temperature of PCM in each layer should gradually decreases along the flowing direction of heat transfer fluid during the charging process, to realize the multi-layered heat storage. The various composite pellets with different PCMs can be fabricated by the proposed low-temperature approach in this study. Another strategy is parallel channels with multi-layered heat storage as shown in Fig. 11(b). In this strategy, a square die is required to produce brick-shape composite HSMs. The resulting composite bricks containing different PCMs are orderly arranged to form multiple parallel channels. The change trend of the melting temperature of PCMs in each brick is the same as that in the packed bed strategy. Thermal insulation can be applied between composite bricks containing different PCMs to decrease thermal mixing. As mentioned in Section 1, the multi-layered heat storage is helpful to reducing exergy loss and increasing operating time [25]. Both the two configurations of proposed packed bed and parallel channels can be easily connected to concentrating solar power system, industrial heat networks and CAES systems, to perform the function of HTTES and thus achieve high-efficiency solar heat utilization, industrial waste heat recovery and round-trip efficiency improvement of CAES systems.

4. Conclusions

This work established for the first time a novel method based on cold sintering for encapsulation of phase change material (PCM) to form shape-stabilized composite heat

storage materials (HSMs). In this method, the shape-stabilized composite HSMs can be formed at an extraordinarily low temperature with the aid of high pressure and transient aqueous solvent, in contrast to the conventional fabrication technologies generally performed at high temperatures. $NaNO_3/Ca(OH)_2$ composite HSMs were exemplified to manifest the feasibility of this method. The highly dense $Ca(OH)_2$ matrix was formed to yield firm three-dimensional network structure and successfully microencapsulate $NaNO_3$ as PCM, thus avoiding the macroscopic deformation of composite and preventing the leakage of PCM during the charging/discharging process. The water solubility of $Ca(OH)_2$ played a critical role in the formation of dense structure, which enabled the utilization of water as solvent during the cold sintering process. The stable shape of the composite HSMs even at superheated temperatures enabled direct contact heat transfer. The experimental observations also suggested that the resulting composite HSMs exhibited reliable phase change performance with little melting temperature shift in the thermal cycling tests, good chemical compatibility between the PCM and matrix, good thermal stability, excellent mechanical properties, high energy storage density and long discharging process of thermal energy. More than a case study of $NaNO_3/Ca(OH)_2$ composite HSMs, the demonstrated approach can also provide a fundamental methodology for the extra-low temperature fabrication of a wide range of shape-stabilized composite HSMs for high temperature thermal energy storage. Such a technique is significantly important since it offers a feasible roadmap for energy-saving, low-carbon and cost-effective fabrication of composite HSMs. Future work would be devoted to optimization of sintering parameters and improvement of thermal properties as well as development of more composite HSMs with various melting temperatures.

The comparative analysis demonstrated that the shape-stabilized composite HSMs prepared by the proposed low-temperature approach in this study offered much higher heat storage capacity than the conventional solid sensible heat storage materials. The former can

be used to substitute the latter in various high temperature thermal energy storage applications. Two configurations with multi-layered thermal storage, packed bed and parallel channel were proposed to perform the high temperature thermal energy storage function of the prepared composite HSMs, which can be easily used to facilitate the utilization of solar heat and improve the overall performance of compressed air energy storage system.

References

[1] Liu M, Steven Tay NH, Bell S, Belusko M, Jacob R, Will G, Saman W, Bruno F. Review on concentrating solar power plants and new developments in high temperature thermal energy storage technologies. Renew Sust Energ Rev 2016;53:1411-32.

[2] Miró L, Gasia J, Cabeza LF. Thermal energy storage (TES) for industrial waste heat (IWH) recovery: A review. Appl Energy 2016;179:284-301.

[3] Peng H, Yang Y, Li R, Ling X. Thermodynamic analysis of an improved adiabatic compressed air energy storage system. Appl Energy 2016;183:1361-73.

[4] Georgiou S, Shah N, Markides CN. A thermo-economic analysis and comparison of pumped-thermal and liquid-air electricity storage systems. Appl Energy 2018;226:1119-33.

[5] Pirasaci T, Wickramaratne C, Moloney F, Goswami DY, Stefanakos E. Influence of design on performance of a latent heat storage system at high temperatures. Appl Energy 2018;224:220-9.

[6] Ma B, Li J, Xu Z, Peng Z. Fe-shell/Cu-core encapsulated metallic phase change materials prepared by aerodynamic levitation method. Appl Energy 2014;132:568-74.

[7] Diao YH, Liang L, Zhao YH, Wang ZY, Bai FW. Numerical investigation of the thermal performance enhancement of latent heat thermal energy storage using longitudinal rectangular fins and flat micro-heat pipe arrays. Appl Energy 2019;233-234:894-905.

[8] Umair MM, Zhang Y, Iqbal K, Zhang S, Tang B. Novel strategies and supporting materials applied to shape-stabilize organic phase change materials for thermal energy storage–A review. Appl Energy 2019;235:846-73.

[9] Ge Z, Ye F, Ding Y. Composite materials for thermal energy storage: enhancing performance through microstructures. ChemSusChem 2014;7:1318-25.

[10] Qin Y, Leng G, Yu X, Cao H, Qiao G, Dai Y, Zhang Y, Ding Y. Sodium sulfate–diatomite composite materials for high temperature thermal energy storage. Powder Technology 2015;282:37-42.

[11] Xu G, Leng G, Yang C, Qin Y, Wu Y, Chen H, Cong L, Ding Y. Sodium nitrate – Diatomite composite materials for thermal energy storage. Sol Energy 2017;146:494-502.

[12] Leng G, Qiao G, Jiang Z, Xu G, Qin Y, Chang C, Ding Y. Micro encapsulated & form-stable phase change materials for high temperature thermal energy storage. Appl Energy 2018;217:212-20.

[13] Huang X, Chen X, Li A, Atinafu D, Gao H, Dong W, Wang G. Shape-stabilized phase change materials based on porous supports for thermal energy storage applications. Chemical Engineering Journal 2019;356:641-61.

[14] Oya T, Nomura T, Okinaka N, Akiyama T. Phase change composite based on porous nickel and erythritol. Appl Therm Eng 2012;40:373-7.

[15] Liu R, Zhang F, Su W, Zhao H, Wang C-a. Impregnation of porous mullite with Na_2SO_4 phase change material for thermal energy storage. Sol Energy Mater Sol Cells 2015;134:268-74.

[16] Goitandia AM, Beobide G, Aranzabe E, Aranzabe A. Development of content-stable phase change composites by infiltration into inorganic porous supports. Sol Energy Mater Sol Cells 2015;134:318-28.

[17] Gao H, Wang J, Chen X, Wang G, Huang X, Li A, Dong W. Nanoconfinement effects on thermal properties of nanoporous shape-stabilized composite PCMs: A review. Nano Energy 2018;53:769-97.

[18] Milián YE, Gutiérrez A, Grágeda M, Ushak S. A review on encapsulation techniques for inorganic phase change materials and the influence on their thermophysical properties. Renew Sust Energ Rev 2017;73:983-99.

[19] Peng H, Zhang D, Ling X, Li Y, Wang Y, Yu Q, She X, Li Y, Ding Y. n-Alkanes Phase Change Materials and Their Microencapsulation for Thermal Energy Storage: A Critical Review. Energy & Fuels 2018;32:7262-93.

[20] Nomura T, Zhu C, Sheng N, Saito G, Akiyama T. Microencapsulation of metal-based phase change material for high-temperature thermal energy storage. Scientific Reports 2015;5:9117.

[21] Yu Q, Romagnoli A, Al-Duri B, Xie D, Ding Y, Li Y. Heat storage performance analysis and parameter design for encapsulated phase change materials. Energy Convers Manage 2018;157:619-30.

[22] Nomura T, Sheng N, Zhu C, Saito G, Hanzaki D, Hiraki T, Akiyama T. Microencapsulated phase change materials with high heat capacity and high cyclic durability for high-temperature thermal energy storage and transportation. Appl Energy 2017;188:9-18.

[23] Kähäri H, Teirikangas M, Juuti J, Jantunen H. Dielectric Properties of Lithium Molybdate Ceramic Fabricated at Room Temperature. J Am Ceram Soc 2014;97:3378-9.

[24] McTigue JD, Castro J, Mungas G, Kramer N, King J, Turchi C, Zhu G. Hybridizing a geothermal power plant with concentrating solar power and thermal storage to increase power generation and dispatchability. Appl Energy 2018;228:1837-52.

[25] Galione PA, Pérez-Segarra CD, Rodríguez I, Torras S, Rigola J. Multi-layered solid-PCM thermocline thermal storage for CSP. Numerical evaluation of its application in a 50MWe plant. Sol Energy 2015;119:134-50.

[26] Huang Z, Luo Z, Gao X, Fang X, Fang Y, Zhang Z. Investigations on the thermal stability, long-term reliability of LiNO3/KCl – expanded graphite composite as industrial waste heat storage material and its corrosion properties with metals. Appl Energy 2017;188:521-8.

[27] Maria J-P, Kang X, Floyd RD, Dickey EC, Guo H, Guo J, Baker A, Funihashi S, Randall CA. Cold sintering: Current status and prospects. Journal of Materials Research 2017;32:3205-18.

[28] Guo J, Guo H, Baker AL, Lanagan MT, Kupp ER, Messing GL, Randall CA. Cold Sintering: A Paradigm Shift for Processing and Integration of Ceramics. Angew Chem Int Ed 2016;55:11457-61.

[29] Funahashi S, Guo J, Guo H, Wang K, Baker AL, Shiratsuyu K, Randall CA. Demonstration of the cold sintering process study for the densification and grain growth of ZnO ceramics. J Am Ceram Soc 2017;100:546-53.

[30] Bouville F, Studart AR. Geologically-inspired strong bulk ceramics made with water at room temperature. Nature Communications 2017;8:14655.

[31] Darkwa J, Su O, Zhou T. Development of non-deform micro-encapsulated phase change energy storage tablets. Appl Energy 2012;98:441-7.

[32] Wang T, Wang S, Geng L, Fang Y. Enhancement on thermal properties of paraffin/calcium carbonate phase change microcapsules with carbon network. Appl Energy 2016;179:601-8.

[33] Jiang B, Wang X, Wu D. Fabrication of microencapsulated phase change materials with TiO_2/Fe_3O_4 hybrid shell as thermoregulatory enzyme carriers: A novel design of applied energy microsystem for bioapplications. Appl Energy 2017;201:20-33.

[34] Gimenez P, Fereres S. Effect of heating rates and composition on the thermal decomposition of nitrate based molten salts. Energy Procedia 2015;69:654-62.

[35] Raade JW, Padowitz D. Development of molten salt heat transfer fluid with low melting point and high thermal stability. J Sol Energy Eng 2011;133:031013.

[36] McTigue JD, White AJ, Markides CN. Parametric studies and optimisation of pumped thermal electricity storage. Appl Energy 2015;137:800-11.

[37] He W, Wang J, Wang Y, Ding Y, Chen H, Wu Y, Garvey S. Study of cycle-to-cycle dynamic characteristics of adiabatic Compressed Air Energy Storage using packed bed Thermal Energy Storage. Energy 2017;141:2120-34.
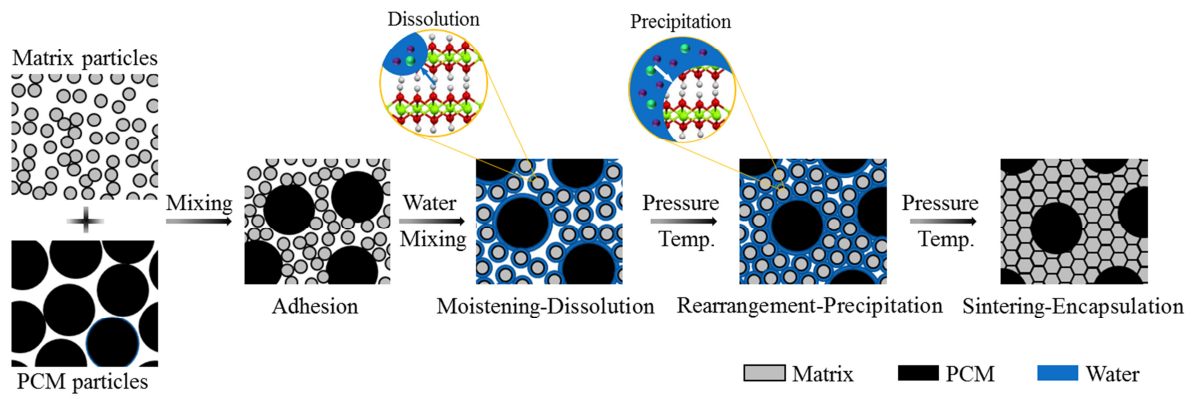
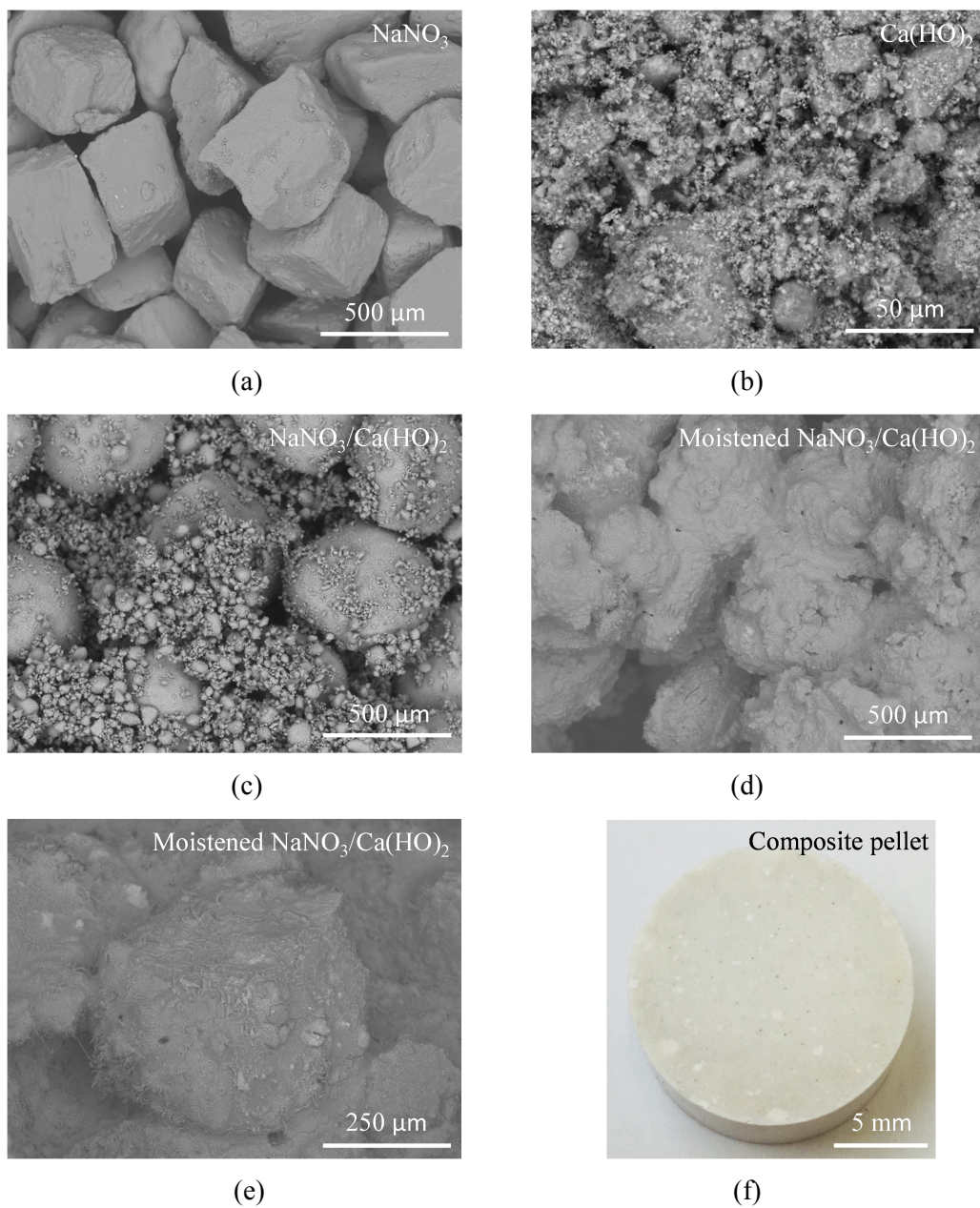Fig. 1 Schematic diagram of cold sintering for producing PCM/matrix composite materials.

Fig. 2 Morphologies of materials at different stages of the fabrication process: (a) NaNO$_3$ particles; (b) Ca(OH)$_2$ particles; (C) NaNO$_3$/Ca(OH)$_2$ mixture particles; (d) moistened mixture particles; (e) close-up view of moistened mixture particles; (f) composite pellet before thermal cycling.

(a)

(b)

Fig. 3 Shapes of composite pellets with $NaNO_3$ as PCM at various sintering temperatures (marked at the bottom of each pellet) after 400-times thermal cycling between 270 °C and 350 °C: (a) $CaCO_3$ as matrix; (b) $Ca(OH)_2$ as matrix.

(a)

(b)

(c)

(d)
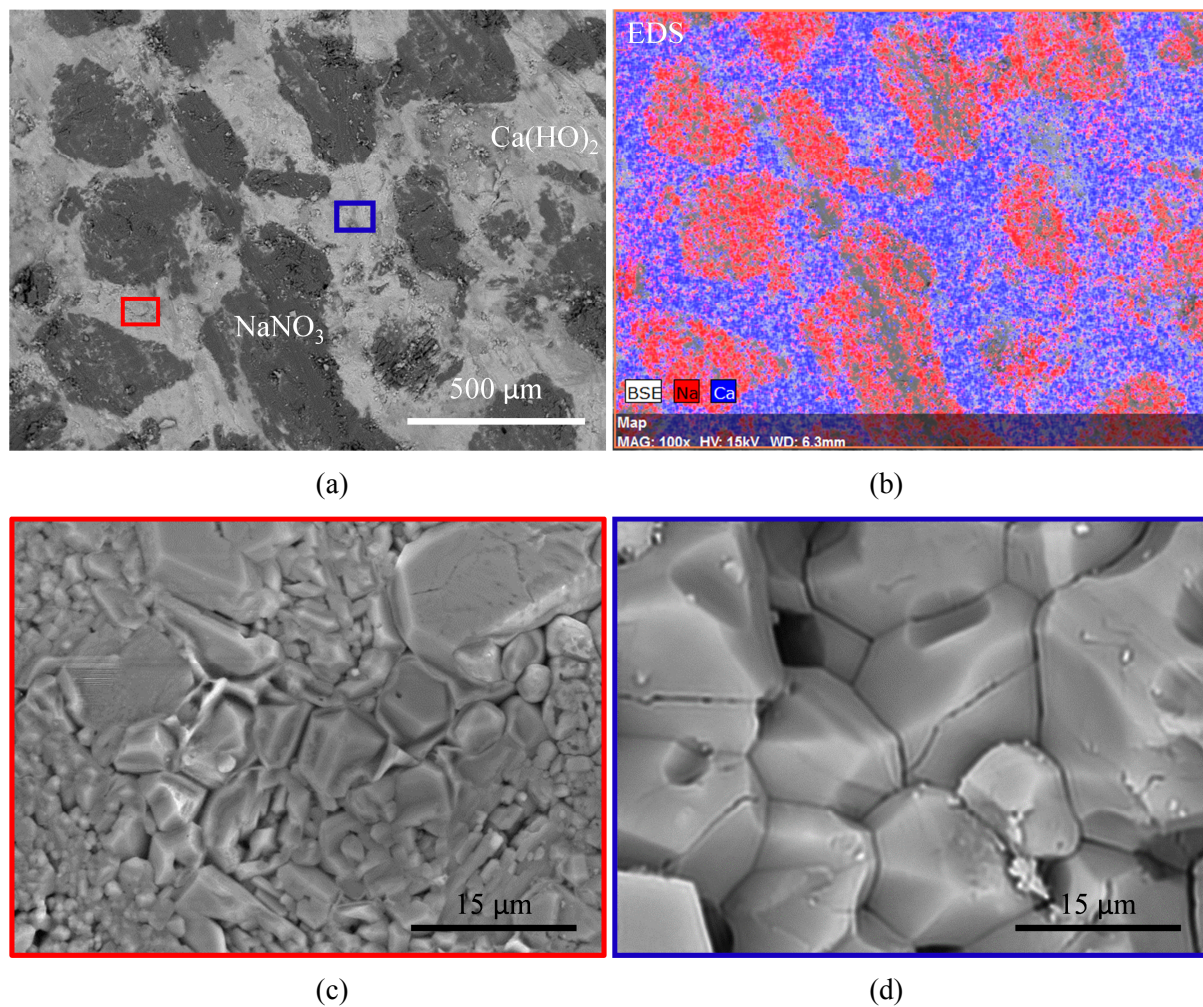
Fig. 4 (a) Microstructure of NaNO₃/Ca(OH)₂ composite sample under SEM; (b) Element map corresponding to (a); (c, d) Local structure in the areas marked by red and blue wireframes in (a).
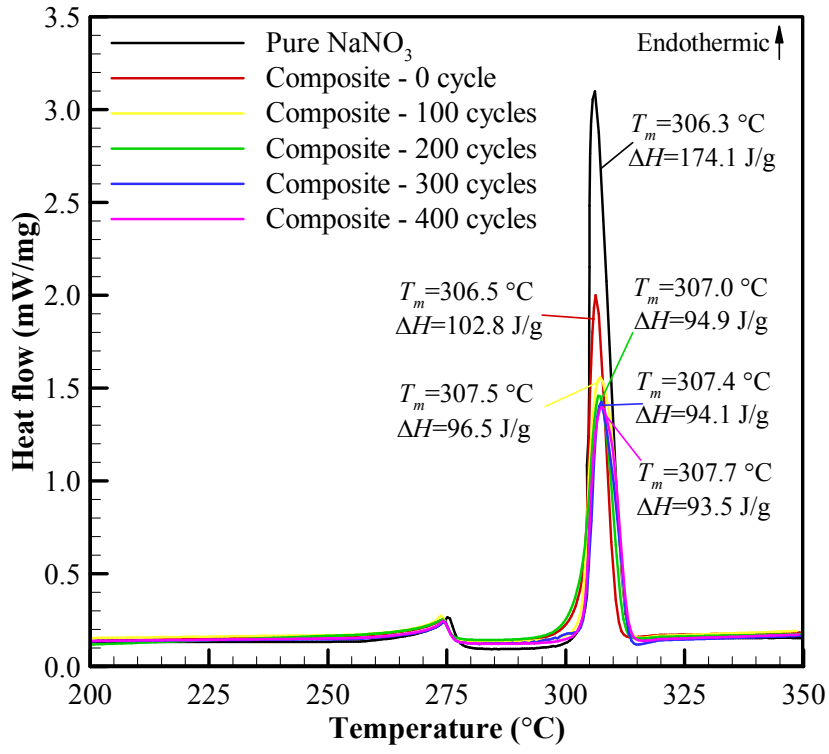
(a)
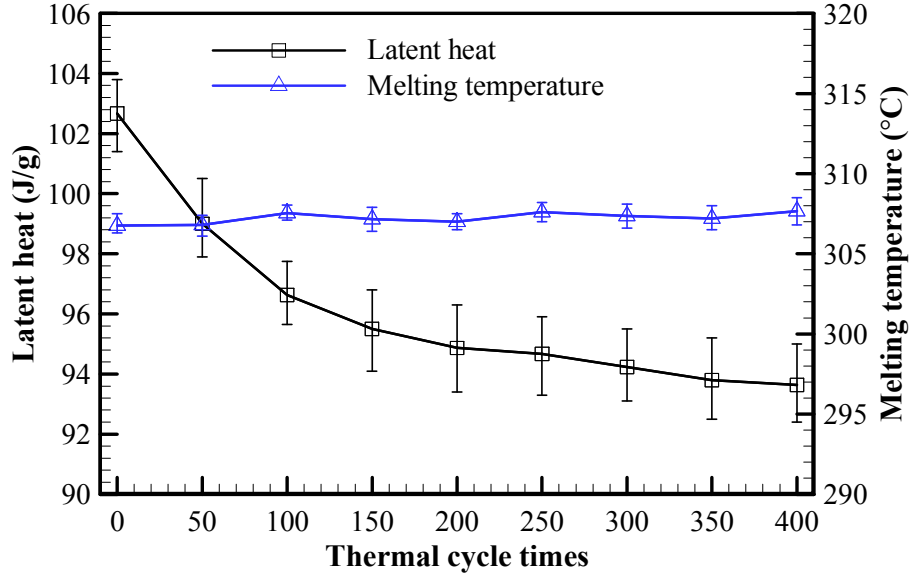
(b)

Fig. 5. Thermal performance of NaNO$_3$/Ca(OH)$_2$ composite samples: (a) DSC curves; (b) variations of latent heat and melting temperature with thermal cycle times. In (a), T_m and ΔH denote the melting temperature (peak temperature) and the latent heat, respectively.
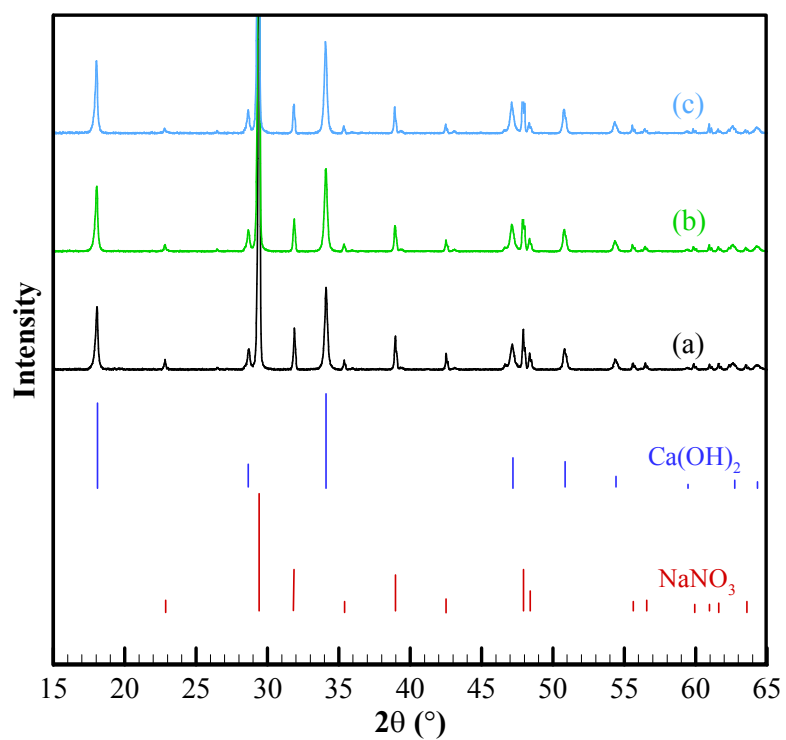
Fig. 6 XRD patterns of NaNO$_3$/Ca(OH)$_2$ composite: (a) before thermal cycling; (b) after 100 thermal cycles; (c) after 200 thermal cycles.
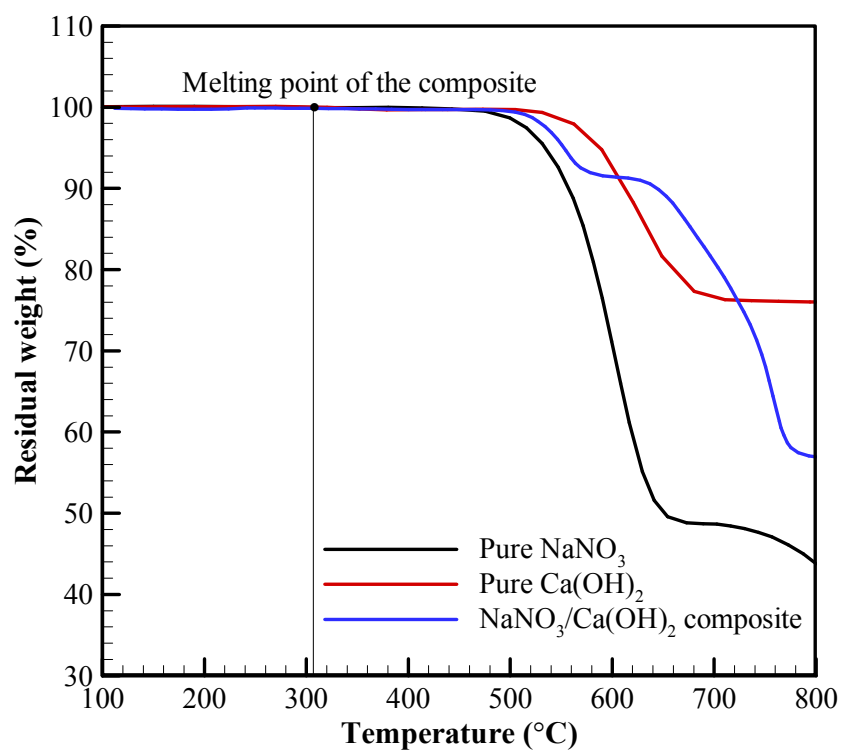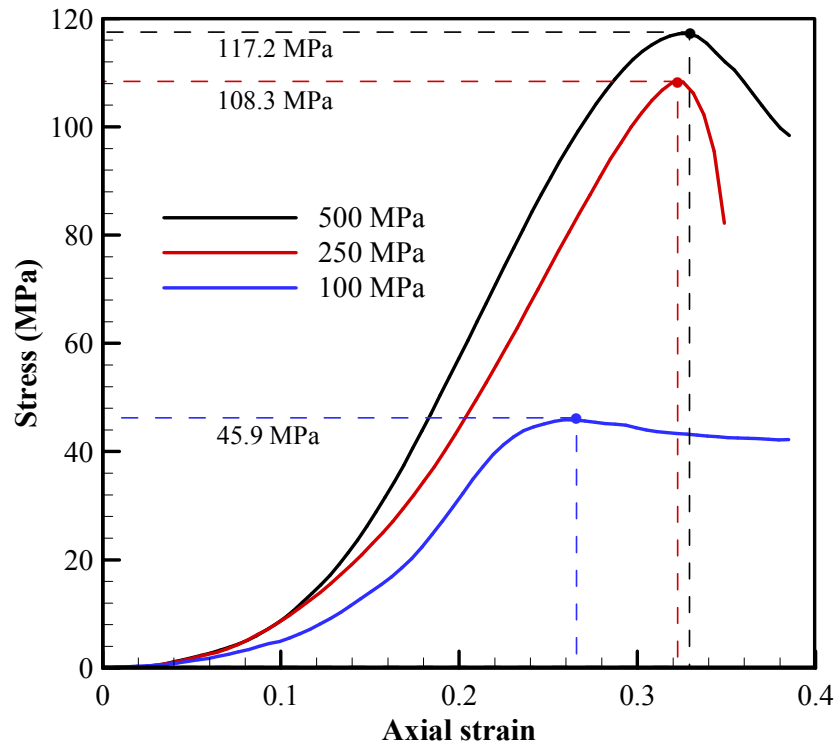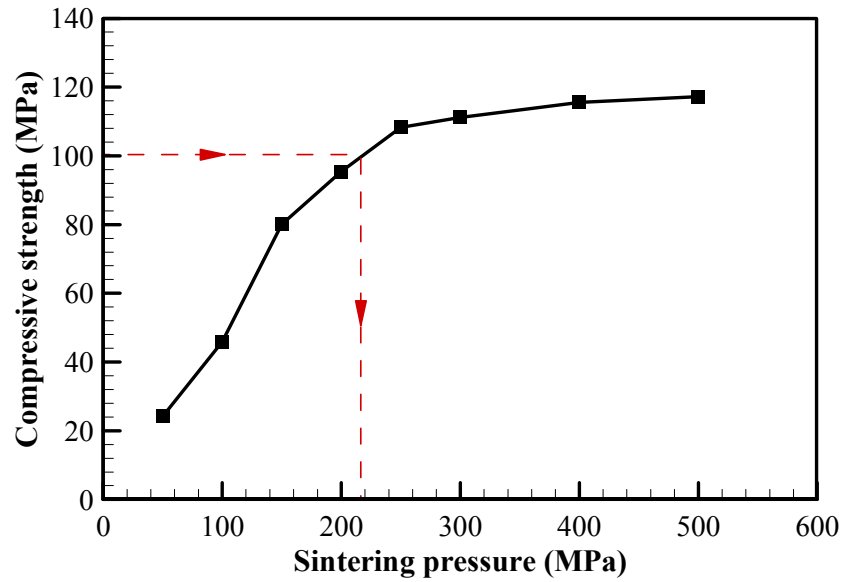
Fig. 7. TGA curves of pure $NaNO_3$, pure $Ca(OH)_2$ and $NaNO_3/Ca(OH)_2$ composite sample.

(a)

(b)

Fig. 8. Mechanical performance of NaNO$_3$/Ca(OH)$_2$ composite pellets: (a) stress-strain curves at different sintering pressure; (b) variation of compressive strength with the sintering pressure.
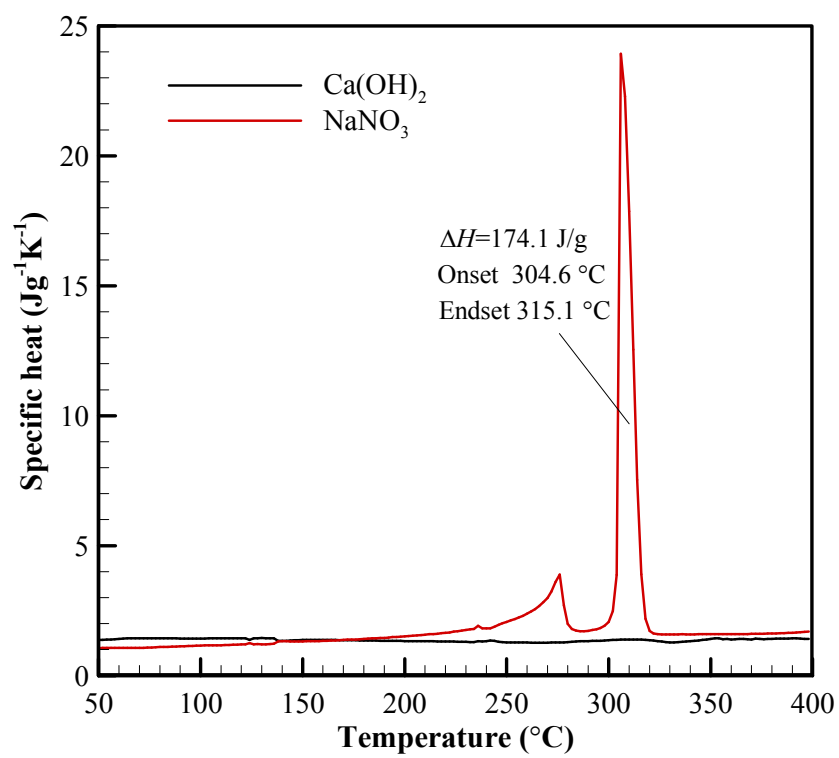
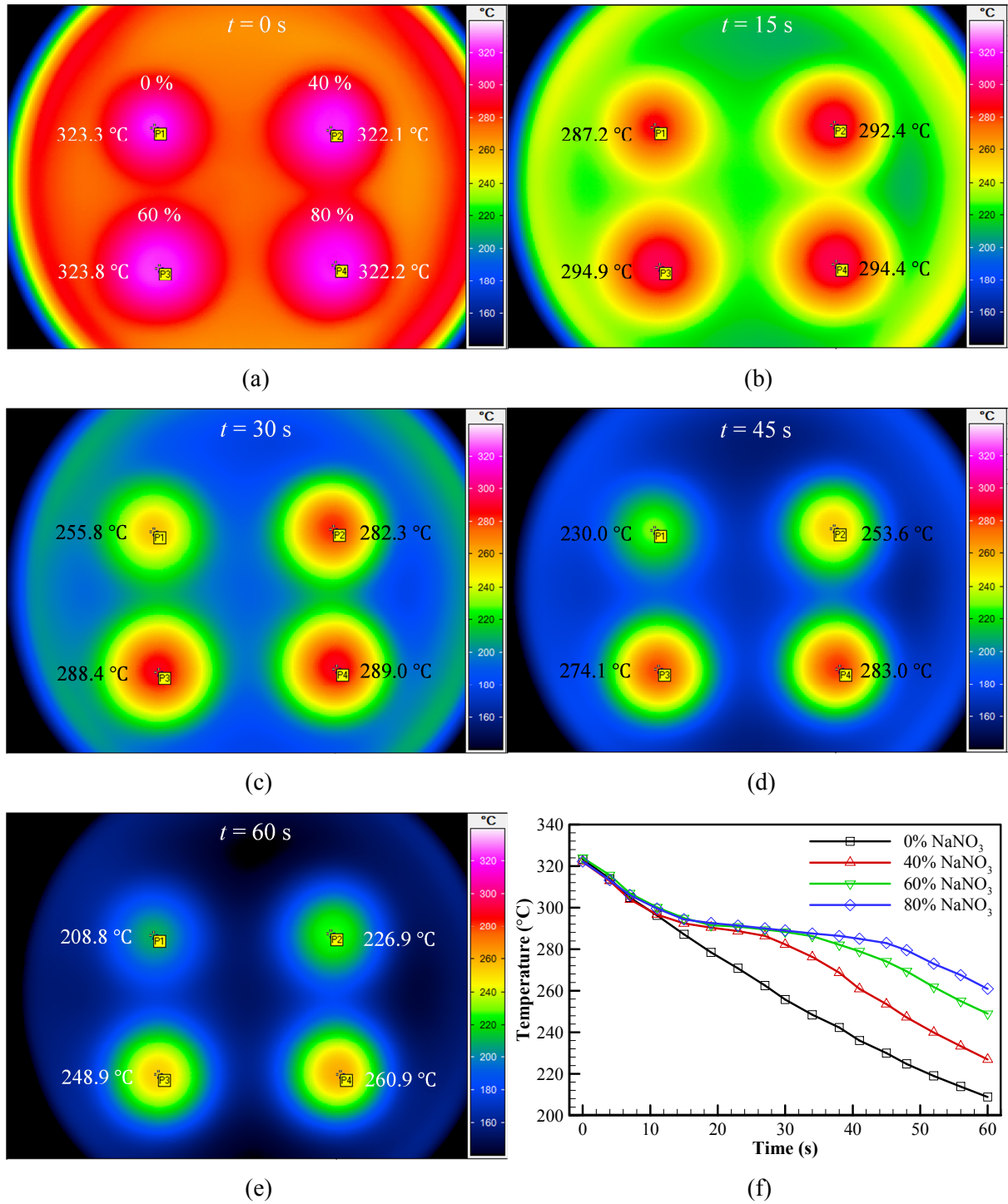Fig. 9 Specific heats of the pure $Ca(OH)_2$ and pure $NaNO_3$.

Fig. 10 Comparison of thermal storage performance between four pellets containing different weight ratios of $NaNO_3$ (0%, 40%, 60% and 80%): (a-e) temperature distributions at different times ($t = 0$ s, 15 s, 30 s, 45 s and 60 s); (e) time-dependent temperature profile at the central point of the upper surface of each pellet. The temperatures at the central points are also marked in (a-e).
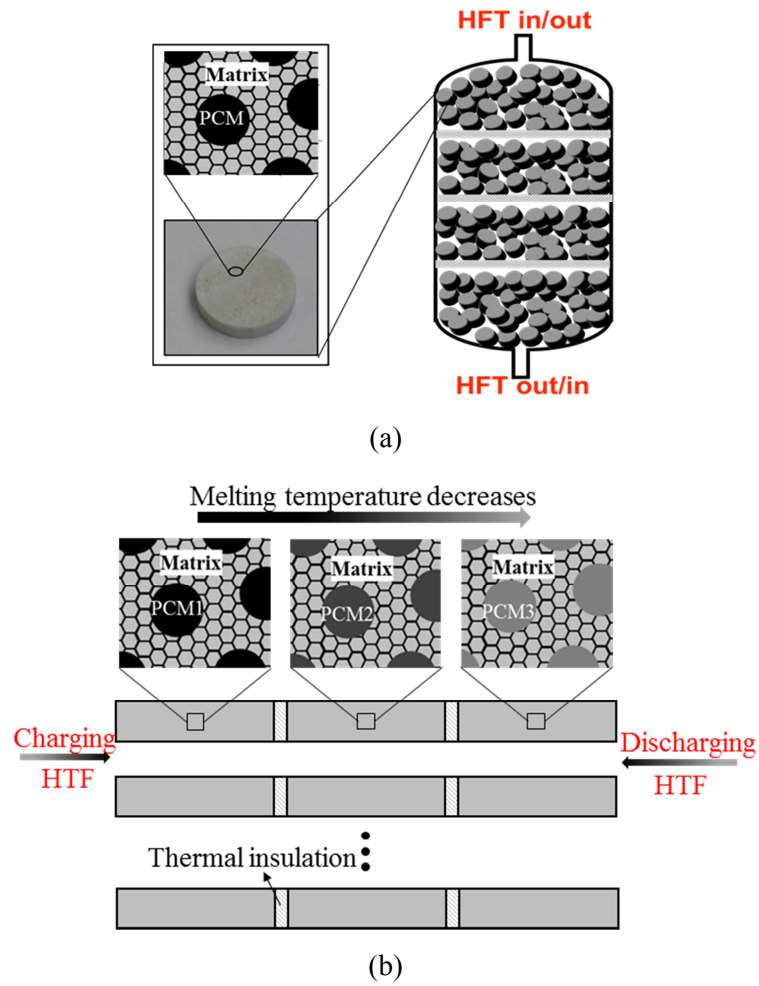
(a)

(b)

Fig. 11 Expected application strategies of prepared shape-stabilized composite HSMs: (a) packed bed;
(b) parallel channels with multi-layered heat storage. HTF denotes heat transfer fluid.

Table 1 Thermal energy storage density and discharging time of composite pellets.

Weight ratio of $NaNO_3$	0%	40%	60%	80%
Thermal energy storage density in the range of 140 ℃–340 ℃ (Jg^{-1})	265.0	366.3	417.0	467.7
Discharging time from 323 ℃ to 140 ℃ (s)	129	142	154	162

Table 2 Comparisons of heat storage capacity of PCM-based shape-stabilized composite HSMs with typical solid sensible heat storage materials of Fe_3O_4 [36] and quartzite [37].

	Unit	Fe_3O_4	Quartzite	PCM-based HSMs with 60 wt.% $NaNO_3$
Temperature range	℃	290-340	290-340	290-340
Specific heat	$J \cdot g^{-1} \cdot k^{-1}$	0.86	0.83	As shown in Fig. 9
Average density	$g \cdot cm^{-3}$	5.175	2.560	2.127
Mass-based heat storage density	$J \cdot g^{-1}$	43.0	41.5	177.2
Volume-based heat storage density	$J \cdot cm^{-3}$	222.5	106.2	376.9